A 3-D resistivity investigation of a contaminated site at Lernacken, Sweden

Dahlin, Torleif; Bernstone, Christian; Loke, MH

Published in:
Geophysics

DOI:
10.1190/1.1527070

2002

GEOPHYSICS, VOL. 67, NO. 6 (NOVEMBER-DECEMBER 2002); P. 1692–1700, 12 FIGS., 1 TABLE.
10.1190/1.1527070

Case History

A 3-D resistivity investigation of a contaminated site at Lernacken, Sweden

Torleif Dahlin*, Christian Bernstone*, and Mong Hong Loke‡

ABSTRACT

A contaminated site at Lernacken in southern Sweden, formerly used for sludge disposal, was investigated using a 3-D resistivity imaging technique. The data acquisition was carried out using a roll-along technique for 3-D data acquisition that allows using standard multielectrode equipment designed for engineering and environmental applications. The technique allows for the measurement of large true 3-D resistivity data sets, and data were measured using two perpendicular electrode-orientation directions with only one layout of the cables. The data were plotted as two sets of pseudo depth slices using the two electrode orientation directions, which resulted in markedly different plots. The complete data set was inverted to form a resistivity-depth model of the ground using a 3-D least-squares smoothness constrained inversion technique. The results obtained were compared to other geophysical and background data, and a good agreement was found. The results show that the 3-D roll-along technique in combination with 3-D inversion can be highly useful for engineering and environmental applications. However, multichannel measurement equipment is necessary to speed up the data acquisition process for routine application.

INTRODUCTION

There is an increasing demand for detailed knowledge about subsurface features in environmental, hydrogeological, and engineering applications. dc resistivity data acquisition is becoming increasingly popular, as the variation in resistivity of the subsurface is often linked to a variation of properties relevant to these applications (e.g., hydraulic properties or the presence of contaminants).

Two-dimensional data acquisition and inversion techniques for dc resistivity surveys have experienced a rapid development over the past years, and often a number of 2-D sections can be merged to form reasonably accurate images of 3-D structures (Dahlin and Loke, 1997; Bernstone et al., 1997). However, in strongly variable environments, 3-D techniques may have to be considered, particularly if detailed mapping of the subsurface structure is required.

For 3-D surveys it is generally unrealistic to employ a data acquisition system that would cover the entire area of interest in one layout, because the number of electrode positions and channels required in the switching device increases by the square of the size of grid investigated. For example, with a switching device having a capacity of 64 channels, only a square of 8×8 electrodes can be covered, which leaves either a small investigated area or a very coarse spatial resolution. This necessitates the use of roll-along techniques.

It would be simple to use a roll-along technique where measurements are taken only in the direction of the cable layout (the x-direction), as illustrated in Figure 1. However, in true 3-D surveys, it is desirable not only to carry out measurements with electrode positions in a fairly dense pattern in both the x- and y-directions, it is also preferable to measure with the electrodes oriented in at least two directions without having to lay out the cables first in one direction and then in the perpendicular direction, due to the cumbersome field logistics. This paper describes a roll-along technique for the acquisition of true 3-D data sets in one pass, with two or more electrode orientations, using a standard switching device with a moderate number of channels.

The large data sets that are generated in a 3-D survey require an automatic 3-D inverse modeling technique in order to extract as much information as possible from the data. This methodology was applied to a survey carried out over a

Manuscript received by the Editor August 17, 1998; revised manuscript received February 6, 2002.
*Lund University, Department of Geotechnology, John Erikssons v. 1, S-223 63 Lund, Sweden. E-mail: torleif.dahlin@tg.lth.se; christian.bernstone@tg.lth.se.
‡University Sains Malaysia, School of Physics, 11800 Penang, Malaysia. E-mail: mhloke@usm.my

contaminated site in southern Sweden. The surveyed area is a former sludge disposal site, where liquid industrial waste was disposed in several shallow ponds. The site was later covered by earth, resulting in a more or less flat surface. The result of the 3-D survey is compared to earlier investigations of the same area using the ordinary 2-D continuous vertical electrical sounding (CVES) technique and electromagnetic profiling.

DATA COLLECTION AND DATA ANALYSIS

Equipment

The data acquisition technique was developed around a multielectrode system designed primarily for engineering and environmental applications, the ABEM Lund Imaging System. The system (see Figure 1) consists of a resistivity meter, a relay-matrix switching unit (Electrode Selector ES464), electrode cables, a computer, steel electrodes, and various connectors (Dahlin, 1996). A modified version of this system was used. The modifications include a separate current amplifier (Booster SAS2000), which transmits the current under direct control from the computer, and a 24 bit A/D converter (Lawson Labs model 201). The latter replaced the resistivity meter and allowed increased control over the measurement process beyond the Terrameter SAS300C that was available at the time of the survey. Eight electrode cables (each having 21 takeouts) with 5-m takeout intervals were used, plus two single-conductor cables for the remote electrodes.

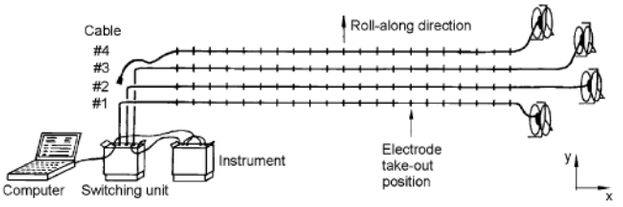

FIG. 1. Sketch of cable layout with roll-along perpendicular to the cable direction.

3-D roll-along technique

The roll-along technique is suitable for emulating electrode grids with a size of up to $32 \times n_y$ with a standard switching device with a maximum of 64 electrodes capacity, where n_y is the number of electrodes in the y-direction. The technique was primarily designed for the pole-pole array, which is the electrode configuration commonly used for 3-D surveys (Loke and Barker, 1996). A pole-pole array will be assumed in the following discussion, but the technique could be adopted for other arrays as well.

Figure 2 is a schematic sketch showing the first three steps in a 3-D roll-along with seven multielectrode cables, where different combinations of two cables at a time are connected to the switching unit. After measuring is finished using one cable pair, the operator has to switch one cable manually before proceeding. After all combinations involving cable 1 are finished and a new cable has been installed ahead of the old cable 7, the cable designation is shifted so that cable 2 becomes cable 1 etc., and the procedure is repeated. Thus, the roll-along procedure can be continued as far as desired. With a total of seven cables up to six times the minimum spacing in the roll-along direction is possible. In this case, an additional cable was used for moving and connecting to electrodes while measuring on the others was in progress.

The available number of cables and electrodes determines the largest practical electrode spacing in the y-direction. For example, a 21×21 grid can be fully covered by measurements in both the x- and y-directions if 21 electrode cables are available. Strictly speaking, only two cables are needed, but this configuration requires the entire cable to be moved instead of switching the connectors between each step in Figure 2, which would make it a very time consuming and work intensive process.

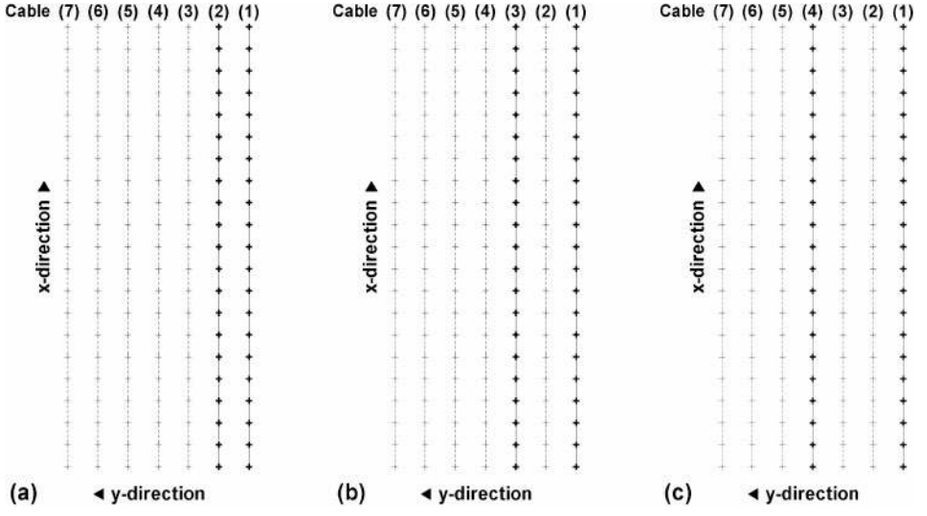

FIG. 2. Sketch showing the first three steps in 3-D roll-along with multielectrode cables, where different combinations of two cables are at the same time connected to the switching unit (the remote electrodes are not shown). Bold lines indicate active cables, the dotted ones are inactive: (a) Cable 1 and cable 2: measuring along both cables and between the two cables. (b) Cable 1 and cable 3: measuring along cable 3 and between the two cables. (c) Cable 1 and cable 4: measuring along cable 4 and between the two cables. The process continues until measurements involving cable 1 and cable 7 are completed, then cable 2 becomes cable 1 and the process is repeated.

With the large arrays being described here, the number of possible electrode permutations is also very large. Using the expression presented by Xu and Noel (1993), we can show that a total of 97 020 independent pole-pole measurements can be taken for the full 21×21 setup. Even if the measurement protocols are reduced to measure the perpendicular x- and y-directions, or if the cross-diagonal strategy suggested by Loke and Barker (1996) is used, the number of individual measurements become large and thus time-consuming to acquire if a single channel instrument is employed. On the other hand, the technique is ideally suited for multichannel measuring, which could speed up the process of surveying tremendously.

3-D inversion method

In order to determine the subsurface resistivity from the measured apparent resistivity measurements, a model that subdivides the subsurface into a number of rectangular blocks was used (Figure 3). The thickness of the top layer was set at 0.5 times the spacing between adjacent electrodes. The thickness for each subsequent deeper layer was increased by 15% because the resolution of the resistivity surveying method decreases with depth (Loke and Barker, 1996). The width of the interior blocks in the top two layers were set at half the unit electrode spacing, while the width of the blocks in the deeper layers were the same as the electrode spacing. In theory, it is possible to use smaller blocks for the lower layers as well in order to improve the model resolution, but this will greatly increase the computer time needed to carry out the data inversion. We have found from tests conducted with synthetic models that the use of smaller blocks does not significantly improve the accuracy of the results, probably because the resolution of surface resistivity surveys decreases with depth. The arrangement used in Figure 3 provides a reasonable compromise between obtaining good model resolution near the surface without excessively increasing the computer time needed.

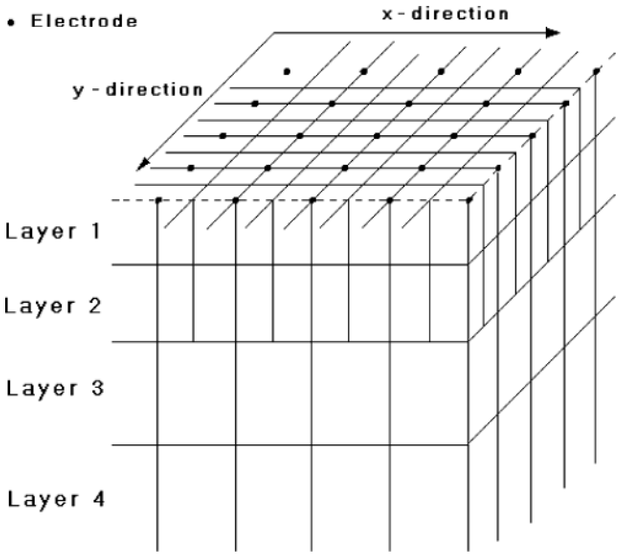

FIG. 3. Division of the subsurface into rectangular blocks. The thickness of the top layer was set at 0.5 times the spacing between adjacent electrodes, and the thickness for each subsequent deeper layer was increased by 15%.

The smoothness-constrained least-squares method (deGroot-Hedlin and Constable, 1990; Sasaki, 1994) was used to determine the resistivity of the blocks in the inversion model for the field data collected. This method is based on the following equation:

$$\left(\mathbf{J}_i^{\mathrm{T}}\mathbf{J}_i + \lambda_i \mathbf{C}^{\mathrm{T}}\mathbf{C}\right)\Delta\mathbf{r}_i = \mathbf{J}_i^{\mathrm{T}}\mathbf{g}_i - \lambda_i \mathbf{C}^{\mathrm{T}}\mathbf{C}\mathbf{r}_{i-1}, \qquad (1)$$

where i is the iteration number, $\mathbf{J}_i$ is the Jacobian matrix of partial derivatives, $\mathbf{g}_i$ is the misfit vector which contains the differences between the logarithms of the measured and calculated apparent resistivity values, and λ_i is the damping factor. The vector $\Delta\mathbf{r}_i$ contains the change in the model resistivity values for the ith iteration, and $\mathbf{r}_{i-1}$ is the model resistivity values for the previous iteration. The roughness filter $\mathbf{C}$ matrix is used to constrain the smoothness of the resulting resistivity model so as to prevent unstable or extreme solutions. The damping factor determines the relative importance given to reduce the data misfit and the smoothness of the model (Ellis and Oldenburg, 1994). The finite-difference method (Dey and Morrison, 1979) was used to calculate the apparent resistivity values as well as the elements of the Jacobian matrix (McGillivray and Oldenburg, 1990) for the inversion model.

FIELD EXPERIMENT: LERNACKEN SLUDGE PONDS

Background and site description

A field experiment was carried out at Lernacken, Malmö, Sweden, over a closed sludge disposal site (Figures 4 and 5). The site is situated in southern Sweden, at the abutment of the Öresund bridge, and has been previously investigated with dc resistivity imaging and electromagnetic profiling (Bernstone and Dahlin, 1998). The data set has been presented by an animated 3-D visualization (described in Bernstone et al., 1997).

The Lernacken area has been extended out in the sea by several hundred meters as a result of 80 years of landfilling. Although few early records about the disposed material exist, it is believed that the materials used were mostly lime quarry waste and excavated soil. In the 1960s, several ponds 1–4 m deep were dug in the fill material for the deposition of sludge waste. After closure of the disposal site in 1987, the waste was covered with glacial till. Sludge from gutter wells, grease and oil from separators, and waste from processing industries make up the waste body (VBB VIAK, 1992a). Soil analysis has revealed very high levels of organic contaminants and heavy metals in the area, with contaminant levels quickly decreasing in the underlying soils. No leakage collection system exists, and chemical

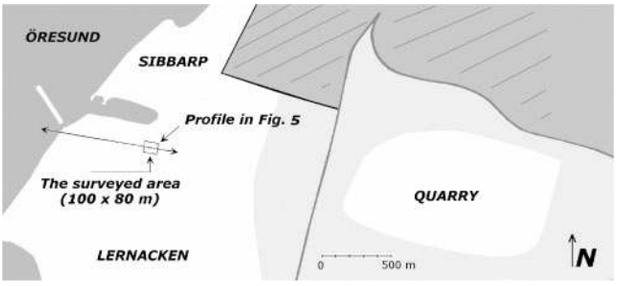

FIG. 4. Lernacken area with the 1995 survey area indicated. The 1996 investigation covered a limited part of the 1995 survey.

analyses of the groundwater have revealed considerably raised levels of several substances. Analyses of three substances are listed in Table 1.

Geology and hydrogeology

The upper bedrock in the region (Figure 5) is Tertiary limestone overlain by a sheet of glacial till, which follows the slightly undulating limestone relief. The transition to harder limestone is often diffuse, passing through a layer of eroded limestone. The thickness of the Quaternary cover ranges between 2 and 15 m, and it is composed mainly of clay tills and stratified interglacial sediments. Locally, especially in the uppermost part, coarser material forms relatively permeable bodies (VBB VIAK, 1992b).

The overall groundwater flow is west northwest towards the sea. The glacial till separates the soil and the regionally important limestone aquifers. Topography and the till barrier cause the buildup of hydraulic pressure in the limestone aquifer, and, hence, the general groundwater leakage pattern is from the limestone through the semipermeable till into the soil aquifer. However, in places there is local downward directed transport as well, as a result of high hydraulic pressure being built up in piles of fill that rise locally above the surrounding ground. In this way, it is possible for contaminated leachate water to reach deeper strata.

Table 1. Content of three chemical substances in the groundwater. Two samples come from the soil aquifer (Rb7901 and Bp16C), and one (Bp16D) from the rock aquifer (see Figure 5 for locations). The last two columns represent soil and rock background values typically found in the region.

	Sampled boreholes			Back ground levels	
Substance	Rb7901 soil aquifer (mg/liter)	Bp16C soil aquifer (mg/liter)	Bp16D rock aquifer (mg/liter)	Fictive 1 Soil aquifer (mg/liter)	Fictive 2 Rock aquifer (mg/liter)
Chloride	1100	2200	660	36	46.1
Ammonium	44	0.08	0.08	0.02	0.18
Lead	97×10^{-3}	$< 1 \times 10^{-3}$	38×10^{-3}	$< 0.5 \times 10^{-3}$	$< 0.5 \times 10^{-3}$

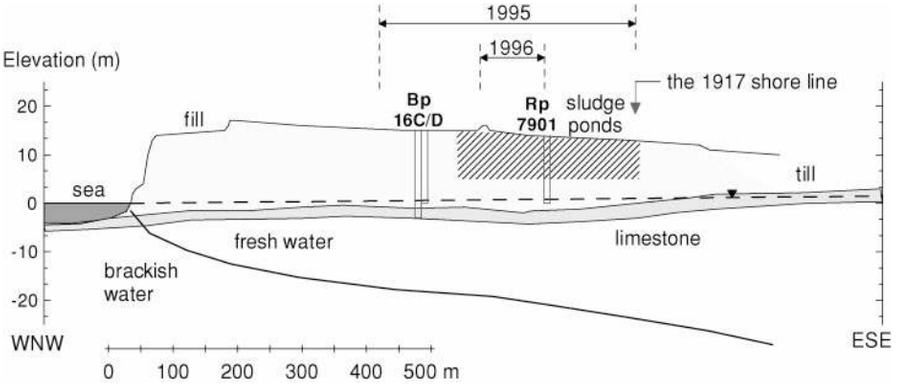

FIG. 5. Cross-section through Lernacken and the sludge pond area. The 1996 label refers to the area where the 3-D roll-along investigation was done, and the 1995 label refers to the 2-D survey which constitute background data for the evaluation of the 3-D resistivity model. Locations of three boreholes are indicated.

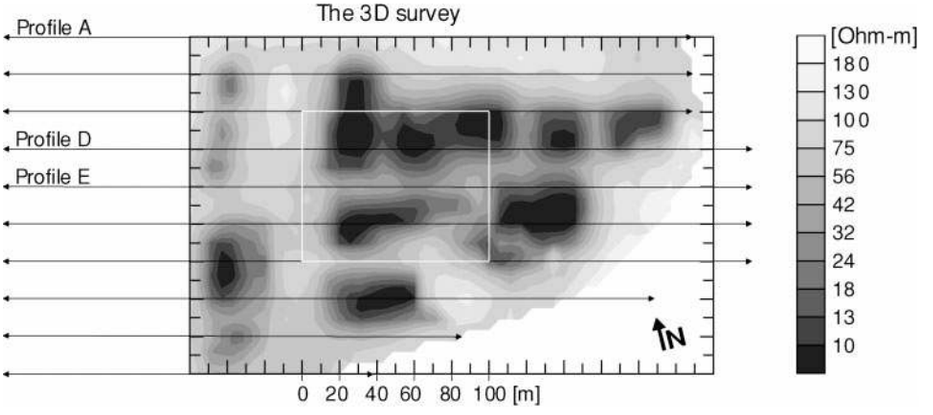

FIG. 6. Contoured EM31 data resolves individual low resistivity ponds. The area of the 3-D survey lies within the white frame, and the arrow lines mark the coverage of the 1995 2-D resistivity surveys, of which profiles A, D, and E (Figure 7) are labeled.

Previous survey (1995)

The apparent resistivities from an earlier slingram survey (using a Geonics EM31) are contoured in Figure 6. Several low resistivity zones are clearly distinguished and correspond to the pond locations, as confirmed by the soil analyses. The measured volume of influence is limited to the upper portion of the saturated soils as inferred by the EM31 cumulative response function. The groundwater level lies at a depth where the contribution to registered conductivities is small.

Three examples of the 2-D inverted Wenner CVES profiles are shown in Figure 7. In profile A, which lies outside the pond area, the upper part of the inverted section is continuous and has a relatively high resistivity. This relatively homogeneous

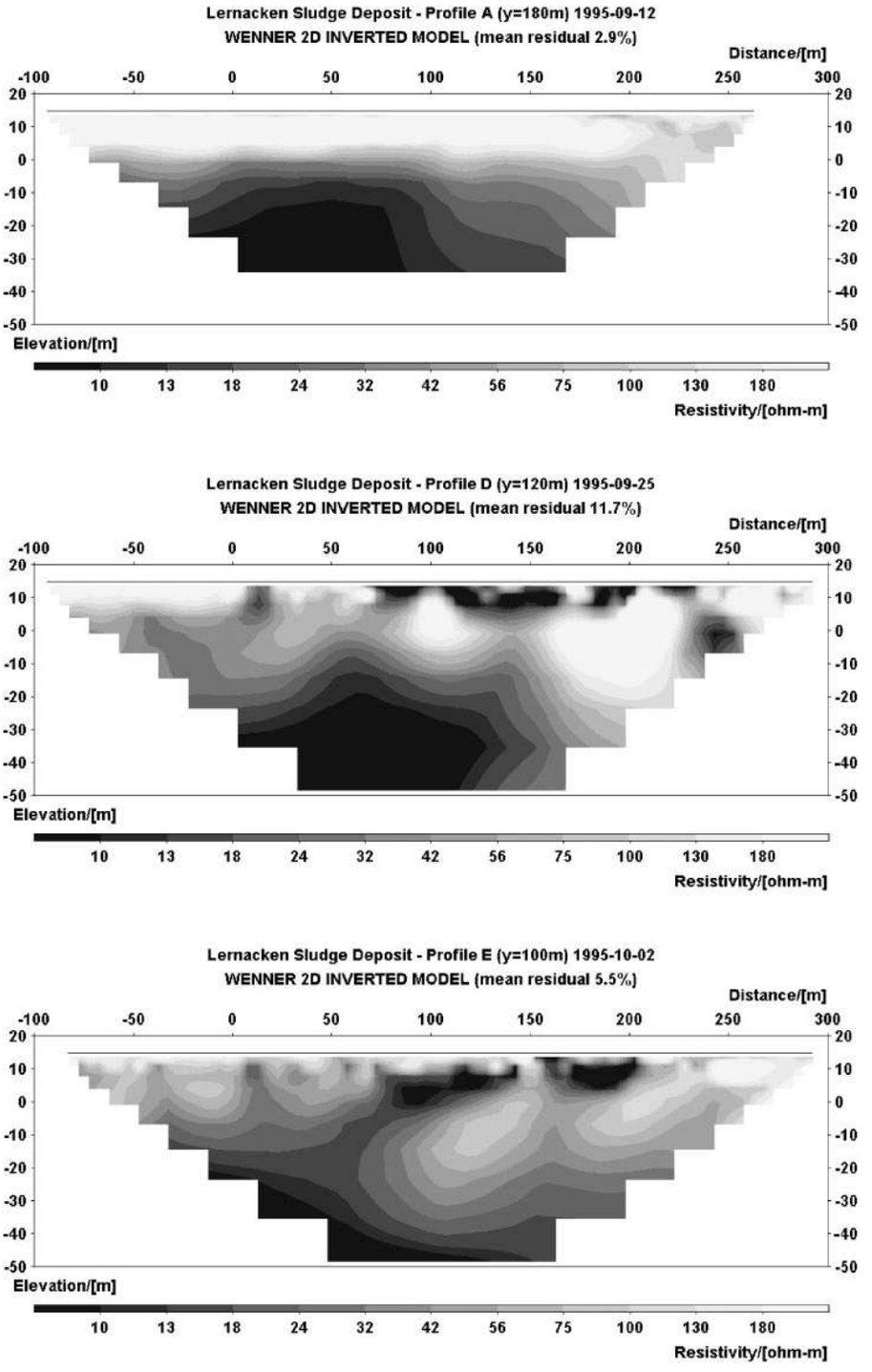

FIG. 7. Three examples of 2-D inverted resistivity models (see Figure 6 for locations) using the Gauss-Newton optimization method. The model fits are 2.9, 11.7, and 5.4%, respectively.

layer corresponds to the fill material, underlain just above sea level by a thin till layer on top of the limestone. The low resistivity in the lower part of the section is interpreted as saline water because the section is measured over the former shoreline of the sea.

The low resistivity zones in the upper parts of profile D and E reflect the disposed waste. The shapes of these zones indicate downward movement of high-conductivity water from the ponds, passing through the fill to (and below) the groundwater table. The low resistivities at the bottom left of these sections are also indicative of saline groundwater due to the sea.

The 3-D survey (1996)

In the 1996 3-D survey, electrode cables were oriented in the x-direction, which is approximately west to east (Figure 8). Each cable covers 100 m between the first and the last takeout, with a 5-m x-spacing. Roll-along measurements using a y-spacing of 5 m were carried out until a grid of 21×17 electrodes was covered. Thus, the total survey area was 100×80 m, and 357 electrode positions were used.

Measurements were only taken in the x- and y-directions, not in the diagonal directions, to limit the time needed for the data acquisition. However, it still took two days to complete the fieldwork. The work was interrupted on several occasions by rabbits biting off the remote electrode cables. Ten and six different electrode spacings were measured in the x-direction and y-direction, respectively (at 1, 2, 3, 4, 5, 6, 7, 8, 9, and 10 times the minimum spacing), which gave a final data set of 3840 data points. The four largest spacings were only used for measurements in the x-direction.

In theory, the pole-pole array has only a single current and potential electrode, commonly referred to as the A and M electrodes, since the connecting electrodes are at infinity. However, in practice, the second current and potential electrodes (referred to as the B and N electrodes, respectively) are located at a finite distance from the survey grid. According to Robain et al. (1997), the distance of the B and N electrodes from the survey grid must be at least 10–20 times the maximum AM distance used so that the measurement array is a sufficiently close approximation to the ideal pole-pole array. This limit corresponds to 500–1000 m in this field survey. Due to the site conditions, the remote electrodes were placed 930 m southwest and 500 m northeast of the survey area. This placement means that the distance requirement is just fulfilled. In the computer inversion of the data set, the effects of remote electrodes were calculated by the finite-difference subroutine used. This minimised any distortion in the results due to these electrodes (Robain et al., 1999).

The background noise levels were checked before measuring began, and the remote electrode with lowest noise level was selected as the potential reference.

RESULTS AND INTERPRETATION

Pseudosections

The resulting data are displayed as pseudodepth slices in two different ways, showing the data taken with the electrodes arranged in the x-direction (Figure 9) and in the y-direction (Figure 10) separately. The pseudodepth slices are based on one electrode separation each, where the apparent resistivity was plotted at the midpoint between the A and M electrodes. Linear interpolation was used for the plotting. Although there is a general agreement between the two directions, in terms of areas of higher and lower apparent resistivities there are significant differences. In particular, a west-east trending band of lower resistivities in the central part of the area is very clearly visible in the y-direction data (Figure 10), but is not obvious in the x-direction (Figure 9). Similarly, some south-north trending features in the northern part of the x-direction data are absent in the y-direction. The low-resistivity areas in the upper pseudoslices correspond to the positions of the former sludge ponds (Figure 6).

3-D inverted model

The data set from the field survey with a 21×17 grid of electrodes has 3840 data points while the inversion model consists of 4800 blocks. The inversion of this data set was carried out on a 550-MHz Pentium III based microcomputer where it took about 6 hours for the program to converge to a satisfactory model.

The resistivity model obtained by the 3-D inversion program is shown as horizontal depth slices in Figure 11a. The inversion process converged after six iterations with a rms misfit of 10.5 for the apparent resistivity values. This value is slightly higher than the misfit for the 2-D models. It could be due to the slightly higher noise level in the pole-pole array measurements in the 3-D survey compared to the Wenner array measurements in the 2-D surveys.

When compared with the results from the slingram and the 2-D resistivity surveys (Figures 6 and 7), it is clear that four

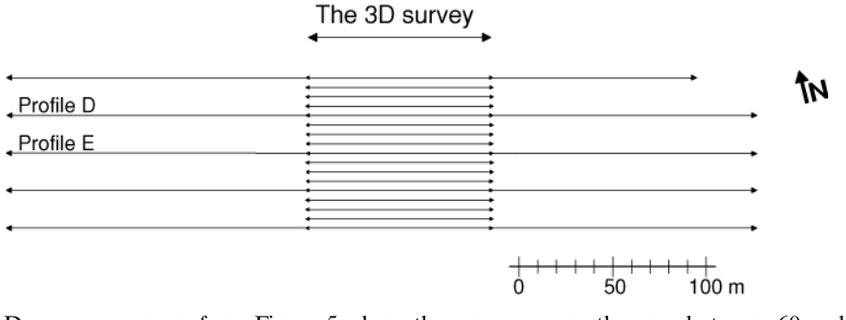

FIG. 8. The 3-D survey coverage from Figure 5 where the survey covers the area between 60 and 160 m, and between the 2-D profiles C-G. The 2-D profiles D and E are included for reference.

low-resistivity ponds are equally well resolved in the top three depth slices of the 3-D resistivity model (Figure 11). The downward movement the conductive leachate solution shown earlier in the 2-D models is also apparent in the 3-D survey model (depth slices 3 and 4). The generally low resistivity values in last two depth slices (8 and 9) are probably due to the influence of conductive seawater.

DISCUSSION AND CONCLUSIONS

The 3-D resistivity imaging technique was successful in delineating contaminated ground, and the technique can be highly useful for engineering and environmental applications. However, in most cases, 2-D techniques without remote electrodes, applied in parallel lines, are probably adequate and are simpler logistically. Such parallel and possibly crossing lines can be inverted using 3-D techniques in complex areas.

The 3-D roll-along technique makes it possible to acquire large data sets with standard multielectrode equipment designed for engineering and environmental applications. With a single-channel instrument, our data acquisition process is very time-consuming, although the technique is well-suited for multichannel measurement techniques, which can reduce the surveying time tremendously.

Obvious practical problems exist when using remote electrodes, one being that long distances are needed for proper layouts. Long distances can be difficult to employ due to logistical constraints from physical barriers. It may be time-consuming to put out the cables, and long voltage bipoles cables are also very sensitive to ambient noise. Furthermore, damage from, for example, animals to the remote cables may cause serious delays, and it is often impossible to continuously guard several kilometers of cable. However, it may be worth overcoming these difficulties when investigating a limited area with the technique described above, especially if a high resolution is required.

The differences in response between the electrode directions can be explained by how the sensitivity function (Frechét derivative) of the array varies in relation to the variation in ground resistivity (Figure 12). If profiling across a highly resistive band at the surface, a negative anomaly will result when the two electrodes are placed on each side of the zone due to the negative sensitivity function between the electrodes. The same effect will not occur when profiling along the zone, because

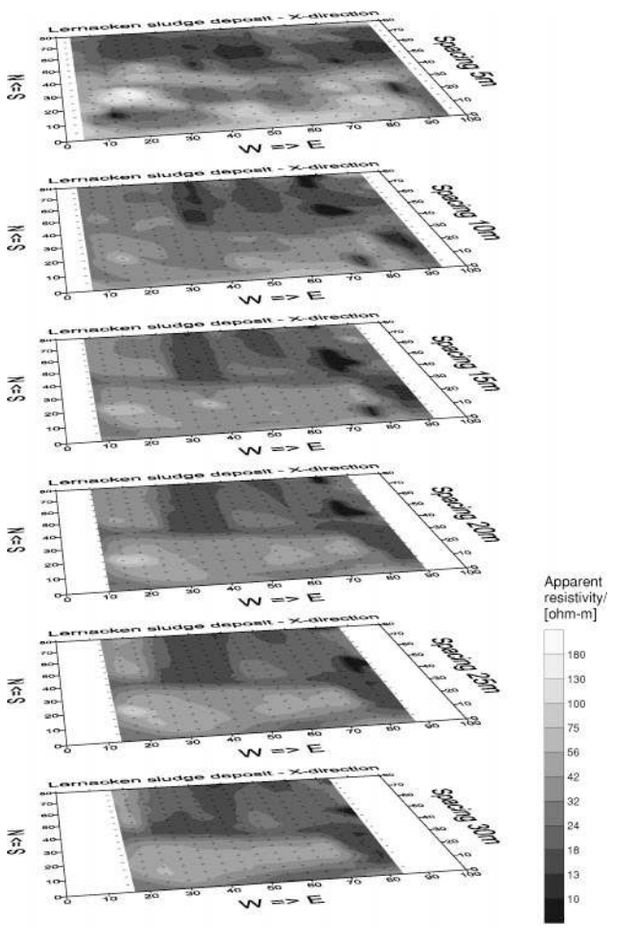

FIG. 9. Pseudodepth slices showing data taken with the electrodes in the x-direction (west-east). Electrode spacings are 5, 10, 15, 25, and 30 m with pole-pole configuration. All distances are in meters.

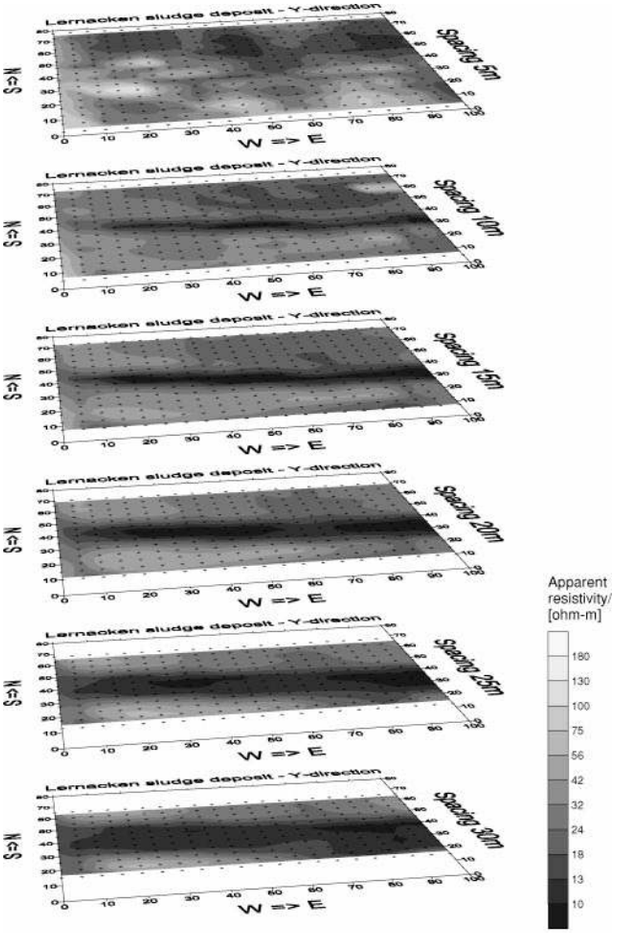

FIG. 10. Pseudodepth slices showing data taken with the electrodes in the y-direction (south-north). Electrode spacings are 5, 10, 15, 25, and 30 m with pole-pole configuration. All distances are in meters.

the positive sensitivities just outside the electrodes will balance the negative zone between them. Thus, the low-resistive band in the lower pseudoslices in the y-direction is an effect of the near-surface area with higher resistivities between the sludge ponds, and not created by any structure at depth. This would be difficult to realize by looking at the pseudodepth plots alone, because the high-resistive band is not clearly visible even in the topmost slices. Similar "shadow effects" appear in the x-direction pseudodepth slices. It is notable that the sensitivities are magnitudes higher for the near-surface variation than for deeper structures (Figure 12), which emphasises the necessity to account for the near-surface variation in order to map the deeper structures.

The 3-D inversion accounts for the effects that depend on the electrode array type and layout direction, because the electrode array characteristics are incorporated in the Jacobian matrix employed in the inversion process. The example clearly demonstrates the necessity of using inverse modeling for the data interpretation, because the pseudoplots can be strongly misleading if used as base for an interpretation of the true structure of the subsurface.

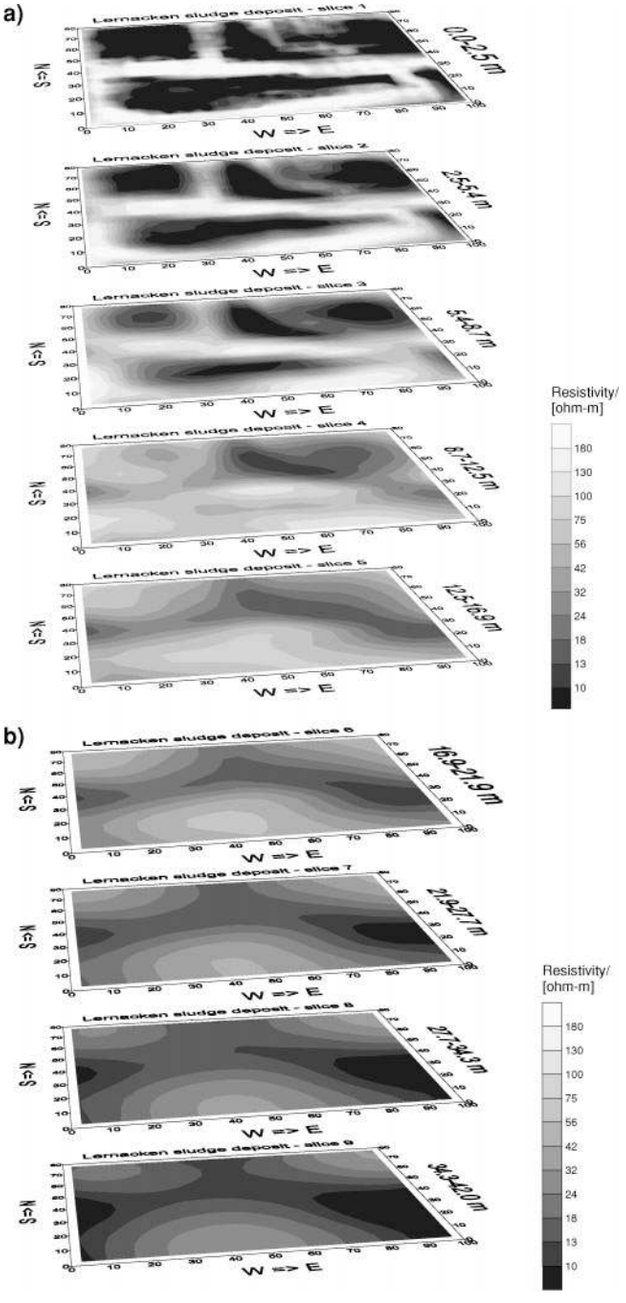

FIG. 11. Inverted depth slices based on all the data. All distances are in meters. (a) Depth intervals 0.0–2.5, 2.5–5.4, 5.4–8.7, 8.7–12.5, and 12.5–16.9 m. (b) Depth intervals 16.9–21.9, 21.9–27.7, 27.7–34.3, and 34.3–42.0 m.

ACKNOWLEDGMENTS

The study has received economic support from the Swedish Geological Survey (SGU), Swedish Environmental Protection Agency (AFN/SNV), and Foundation for Technology Transfer in Lund, which is gratefully acknowledged. We thank SVEDAB (Svensk-Danska Broförbindelsen AB) for fruitful cooperation in connection with the field experiment. Thanks also to Jörgen Brorsson and Ulrika Lerjefors for the gathering of information on the Lernacken area. Thanks to Ingelise Møller for providing Figure 12.

REFERENCES

Bernstone, C., and Dahlin, T., 1998, Electromagnetic and dc resistivity mapping of waste deposits and industrial sites—Experiences from southern Sweden: Eur. J. Eng. Env. Geophys., **2**, 121–136.

Bernstone, C., Dahlin, T., and Jonsson, P., 1997, 3D visualisation of a resistivity data set—An example from a sludge disposal site: Symp. Appl. Geophys. Eng. Environ. Probl., Procs., 917–925.

Dahlin, T., 1996, 2D resistivity surveying for environmental and engineering applications, First Break, **14**, 275–283.

Dahlin, T., and Loke, M. H., 1997, Quasi-3D resistivity imaging: Mapping of 3D structures using two dimensional dc resistivity techniques, 3rd Mtg., Environ. Eng. Geophys. Assn., Expanded Abstracts, 143–146.

deGroot-Hedlin, C., and Constable, S. C., 1990, Occam's inversion to generate smooth, two-dimensional models from magnetotelluric data, Geophysics: **55**, 1613–1624.

Dey, A., and Morrison, H. F., 1979, Resistivity modeling for arbitrarily shaped three-dimensional shaped structures, Geophysics, **44**, 753–780.

Ellis, R. G., and Oldenburg, D. W., 1994, Applied geophysical inversion: Geophys. J. Internat., **116**, 5–11.

Loke, M. H., and Barker, R. D., 1996, Practical techniques for 3D resistivity surveys and data inversion: Geophys. Prosp., **44**, 499–523.

McGillivray, P. R., and Oldenburg, D. W., 1990, Methods for calculating Frechet derivatives and sensitivities for the non-linear inverse problem: A comparative study: Geophys. Prosp., **38**, 499–524.

Møller, I., 1996, Fast approximate 2D inversion of dc-resistivity data: Unpubl. progr. rep., Dept. of Geophysics, Aarhus University.

Park, S. K., and Van, G. P., 1991, Inversion of pole-pole data for 3-D resistivity structures beneath arrays of electrodes: Geophysics, **56**, 951–960.

Robain, H., Alouy, Y., Dabas, M., Descloitres, M., Camerlynck, C., Mechler, P., and Tabbagh, A., 1999, The location of infinite electrodes in pole-pole electrical surveys: Consequences for 2D imaging: J. Appl. Geophys., **41**, 313–333.

Sasaki, Y., 1994, 3-D resistivity inversion using the finite-element method: Geophysics, **59**, 1839–1848.

VBB VIAK, 1992a, Mapping and evaluation of contamination in ground and groundwater at Lernacken—Environmental impact assessment for the Öresund Link (in Swedish): Öresundskonsortiet Report 19.

——— 1992b, Natural resources and land interests within the bridge zone, southern Malmö (in Swedish): Öresundskonsortiet Report 20.

Xu, B., and Noel, M., 1993, On the completeness of data sets with multielectrode systems for electrical resistivity survey: Geophys. Prosp., **41**, 791–801.

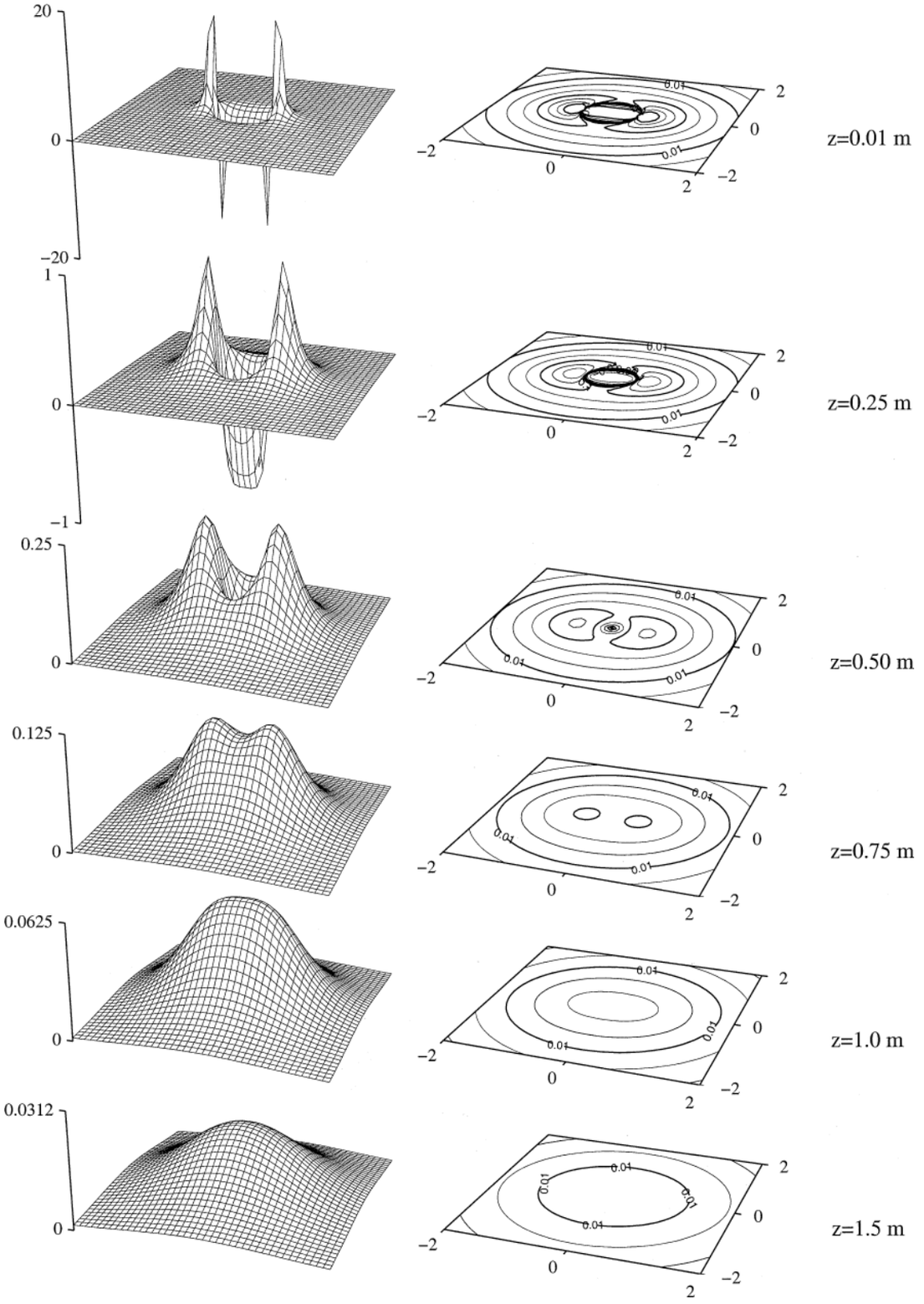

FIG. 12. The 3-D sensitivity function (Frechét derivative) of normalised apparent resistivity for the pole-pole array with a pole-pole distance of 1 m presented as horisontal depth slices at $z = 0.01$, 0.25, 0.5, 0.75, 1.0, and 1.5 m. The electrodes are located at $(-0.5, 0, 0)$ m and $(0.5, 0, 0)$ m. Each slice is shown as a surface plot and a contoured picture. The same logarithmic scale with three intervals per decade is used in the contouring of all slices, but the vertical axis in the surface plots is changed as the maximum of the Frechét derivative decreases rapidly with depth. All distances are in meters. Figure from Møller (1996).